**InComTech: Jurnal Telekomunikasi dan Komputer**
vol.14, no.2, Agustus 2024, 140-152
http://publikasi.mercubuana.ac.id/index.php/Incomtech
P-ISSN: 2085-4811 E-ISSN: 2579-6089

# A Computational Exploration of Electromagnetic Characteristics in Magneto-dielectric Materials

Yohanes Galih Adhiyoga[1*], Tri Nur Arifin[2], Erfiana Wahyuningsih[3], Ganjar Febriyani Pratiwi[4], Margono Sugeng[5]

[1]*Research Center for Telecommunication, National Research and Innovation Agency (BRIN), Jl. Sangkuriang 10, Coblong, Bandung 40135, Indonesia*
[2,3,4]*Electrical Engineering Department, Universitas Dian Nusantara, Jl. Tanjung Duren Barat II No. 1, Jakarta Barat 11470, Indonesia*
[5]*Mechanical Engineering Department, Universitas Dian Nusantara, Jl. Tanjung Duren Barat II No. 1, Jakarta Barat 11470, Indonesia*
*Corresponding author: yoha019@brin.go.id

***Abstract***
Using various new materials in current technological developments not only provides opportunities for better product development but also opens research opportunities in the field of materials science. In the past decade, magneto-dielectric materials have been extensively researched for use in various high-frequency spectrum applications. Before these materials can be widely implemented, their characteristics must first be identified. This paper proposes a process for characterizing the electromagnetic properties within the high-frequency spectrum. Through mathematical analysis conducted via simulations and formula derivation, the relative permittivity, relative permeability, and losses have been successfully identified. Based on experimental results utilizing nine samples for each parameter variation, it is observed that all samples exhibit values identical to the calculated results from the proposed formulas. With its capability to measure dielectric and magnetic properties, this sensor provides a solution for exploring the characteristics of magneto-dielectric materials, which are dominant in both properties.



***Keywords***:
*EM characterization;*
*magneto-dielectric material;*
*permittivity;*
*permeability;*
*FDTD method*

***Riwayat Artikel:***
Diserahkan 11 Desember, 2023
Direvisi 16 Mei, 2024
Diterima 30 Juli, 2024

**DOI**:
10.22441/incomtech.v14i2.24706

## 1. INTRODUCTION

The progress of technology can be seen from advancements in materials research [1]–[4]. Many new technologies have emerged due to the discovery of new materials with unique characteristics. Consequently, many researchers are competing to develop and synthesize new materials with specific desired properties.

For example, Peng introduced derivatives such as graphene, graphdiyne, graphone, and graphene [5]. Materials are now considered both complementary components and primary parameters in determining effectiveness for specific applications. Sreenilayam [6] summarizes various materials suitable for healthcare applications, emphasizing their flexibility and potential for use in wearable devices. In the microwave region, numerous new materials have been introduced and are widely used for applications such as microwave shielding, microwave absorbers [7], and microwave sensors [8], [9]. These materials hold significant potential, yet often, research findings are limited to single-use cases due to constraints in exploring their properties more deeply.

To utilize a material in multiple applications, its characteristics must be thoroughly understood. Detailed knowledge of a material's properties can be obtained by observing high-frequency anomalies using a sensor with characterization capabilities [10]–[12]. Such sensors can be developed through various characterization methods, one of which is the transmission line method, widely used for measuring material properties [13]–[17]. These anomalies can manifest as changes in resonant frequency and quality factor, depending on the material's characteristics. Alamsyah successfully utilized a T-shaped resonator microstrip antenna as a sensor to convert changes in scattering parameters into the permittivity values of solid materials [18], [19]. This change allows the measurement of shifts in scattered parameters to estimate dielectric and magnetic properties.

This paper proposes a numerical computational method to process data on frequency anomalies and the Q-factor of materials into values of permittivity, permeability, dielectric losses, and magnetic losses. We use Finite-Difference Time-Domain (FDTD) simulation software because of its advantage in solving electromagnetic problems. This method directly simulates the behavior of electromagnetic fields over time and space using discrete grids. Unlike the Method of Moments (MoM), which discretizes only the conducting surfaces, and Finite Element Method (FEM), which discretizes the entire domain into elements, FDTD discretizes both space and time. This unique feature allows FDTD to capture transient and time-varying electromagnetic phenomena accurately. The resonant frequency and Q-factor data processed by the software were obtained using a sensor constructed from a microstrip structure designed to distribute electric and magnetic field strengths separately. These field strengths represent the material's dielectric and magnetic properties, which become apparent when the material is placed in the respective regions.

## 2. METHODS

In this study, the material characterization process went through several stages, including sensor design and analysis of simulation results. During the design stage, the field distribution was the basis for selecting the resonator's shape, ensuring that areas with high electric and magnetic fields could be used as permittivity and permeability sensing areas, respectively. In the subsequent stage, the designed sensor was simulated to obtain the frequency response of the material under test

(MUT). This response can then describe the relative permittivity ($\varepsilon_r$) and relative permeability ($\mu_r$).

### 2.1 Microstrip Sensor

In the process of characterizing at high frequencies, some data that can describe the characteristics of the material is taken from the scattered parameters, such as the reflection coefficient ($S_{11}$) and transmission coefficient ($S_{12}$). The proposed sensor has two faces: on the front is a complementary split ring resonator (CSRR) structure, while on the back is a transmission line. S-Parameters data is obtained from the port connected to two ports through the transmission line (Fig. 1).

The sensing process was carried out by dividing the sensor area into two parts: one with high electric field strength and the other with high magnetic field strength. The magnetic field is known to be low in regions with a high electric field, making these regions suitable for permittivity sensing. Conversely, regions with a high magnetic field have a low electric field, making these areas suitable for permeability sensing. Based on this concept, a microstrip sensor was designed to create these two distinct areas. An electric field can be generated through a capacitive element, while a magnetic field can be generated through an inductive element.

Figure 1a shows a front view of a microstrip sensor with two overlapping rectangular resonators. The larger outer resonators have a pattern resembling a capacitor symbol at the ends, indicating areas of high magnetic fields, while the smaller inner resonators indicate areas of high electric fields. These two regions are where the MUT is to be placed. To ensure high sensitivity in these regions, it is essential to verify that they are in the expected condition, which can be done by simulating the field distribution. The simulation results are shown in Figures 2a and 2b.

Measurements were conducted by evaluating the transmission response of the material ($S_{12}$) within these two specified regions, as detailed in our previous investigation [20]. These designated regions are specifically engineered to concentrate the high E-field and H-field exclusively within their respective domains. In regions characterized by elevated E-field levels, the H-field exhibits lower values (Fig. 2a), and conversely, in regions where the H-field is prominent, the E-field diminishes (Fig. 2b). In regions with heightened E-field strengths, we can obtain $S_{21}$ data, which will subsequently be employed for the determination of εr and tan δe values. Conversely, in regions marked by elevated H-field strengths, we can gather $S_{21}$ data to facilitate the calculation of $\mu_r$ and $tan\ \delta_m$ values in subsequent analysis.

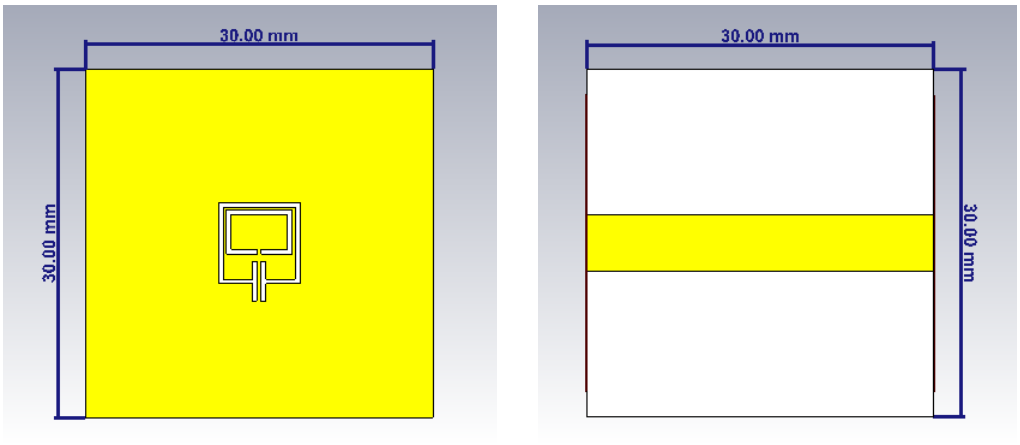


(a) (b)

Figure 1. Microstrip sensor design: (a) Front view and (b) Back view

## 2.2. S-Parameter Simulation

First, the transmission and reflection responses were simulated without the sample to ensure our sensors fit the target frequency. The simulation was conducted using CST Microwave Studio, focusing on the parameters $S_{11}$ and $S_{21}$. The simulation results are shown in Figures 3a and 3b. From the transmission and reflection responses, it is observed that the sensor operates at a frequency of 3.07 GHz, where $S_{11}$ reaches its highest value and $S_{21}$ its lowest level.

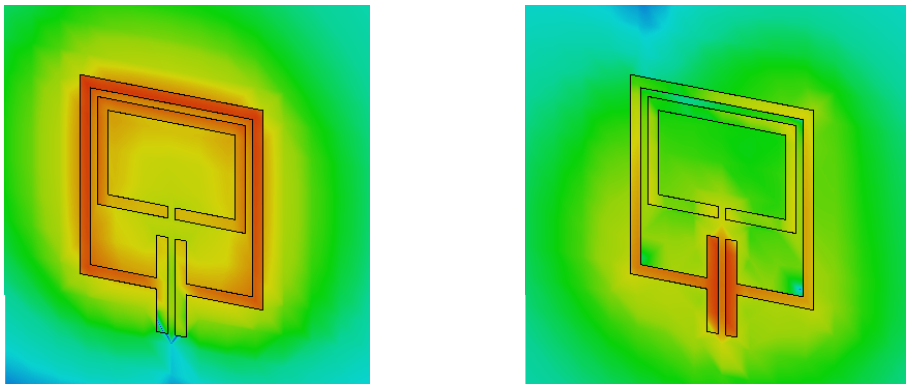

(a) (b)

Figure 2. Field distribution on proposed microstrip sensors: (a) E-field and (b) H-field

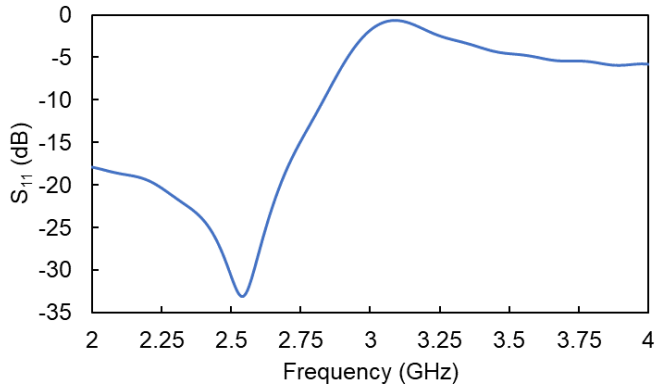


(a)

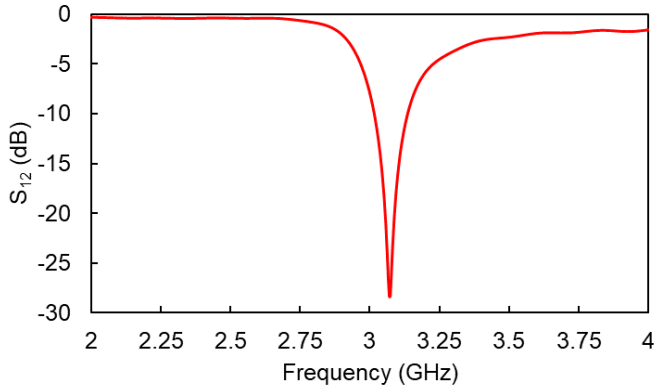


(b)

Figure 3. Scattered parameters of the proposed sensor in the targeted frequency: (a) Reflection coefficient ($S_{11}$), and (b) Transmission coefficient ($S_{12}$)

## 3. RESULTS AND DISCUSSION

### 3.1. Parametric Study Analysis

The extraction process was divided into two parts: calculations to obtain $\varepsilon_r$ and $\mu_r$ values, as well as calculations to obtain $tan\ \delta_e$ and $tan\ \delta_m$ values. Calculations of $\varepsilon_r$ and $\mu_r$ were based on shifts in the resonant frequency, while calculations of $tan\ \delta_e$ and $tan\ \delta_m$ were based on changes in the value of the quality factor (Q-factor) when the MUT was placed in the sensing area [21]. The resonant frequency and Q-factor are then compared with the sensor's resonant frequency and Q-factor when it is still empty without adding MUT.

The first simulation was done by placing the MUT in the dielectric properties sensing area to determine the characteristics of the dielectric material, as shown in Fig. 4a.

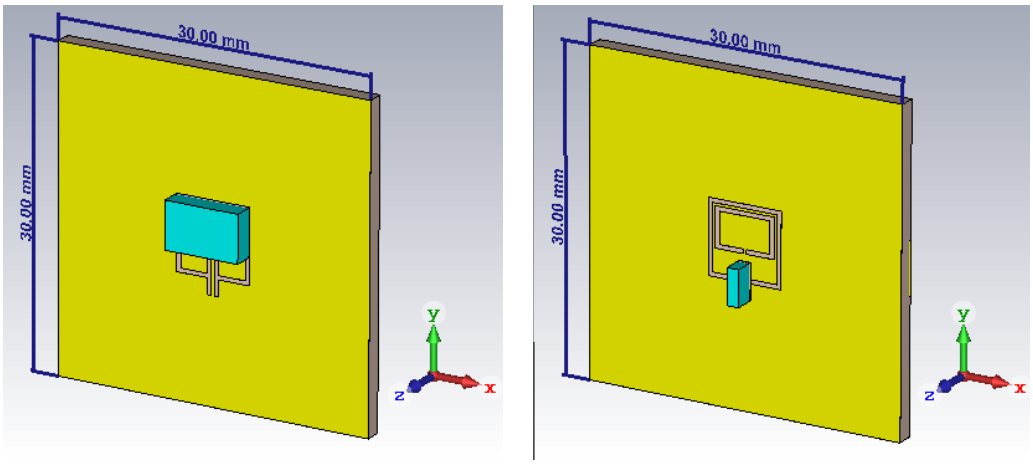


(a) (b)

Figure 4. Sample placement in the sensor to measure (a) Dielectric properties, (b) Magnetic properties

Furthermore, the sample was placed in the other sensing area to measure the magnetic properties (Fig. 4b). We conducted simulations for each sensing region using 18 samples. These simulations involved altering the values of $\varepsilon_r$ and $tan\ \delta_e$, or $\mu_r$ and $tan\ \delta_m$. During the parametric investigations, we maintained a constant value for one of the parameters while changing the other. Subsequently, the resonant frequency and Q-factor for each sample of the MUT were recorded.

By altering the values of $\varepsilon_r$, $\mu_r$, $tan\ \delta_e$, and $tan\ \delta_m$, we acquired the transmission coefficient ($S_{21}$) as depicted in Fig. 5 for dielectric measurement and Fig. 6 for magnetic measurement. The outcomes reveal that when the $\varepsilon_r$ and $\mu_r$ of the MUT are increased, the resonant frequency shifts towards the lower end, indicating a decrease in frequency (Fig. 5a and 6a). Furthermore, it is evident that with higher values of $tan\ \delta_e$ and $tan\ \delta_m$, the Q-factor decreases (Fig. 5b and 6b). In the simulation process, several samples were used, each with different magnetic and dielectric characteristics. These material samples were synthesized by changing the intrinsic parameters of the material to match the expected characteristics. This method predicts the trend the sensor will generate when an unidentified MUT is placed in the sensor area, as discussed in [22] and [23].

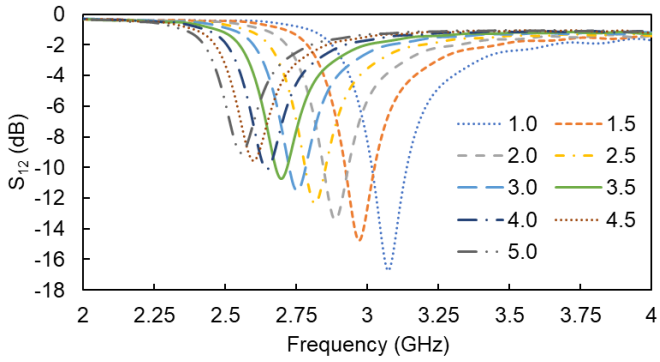


(a)

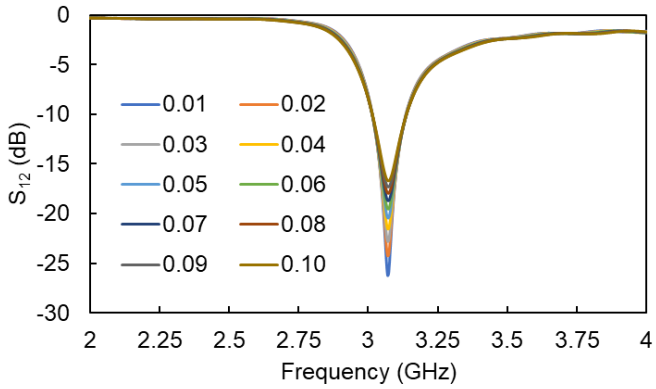


(b)

Figure 5. $S_{12}$ response to changes in (a) $\varepsilon_r$ and (b) *tan* $\delta_e$ in MUT placed in the high E-field area

Figures 5b and 6b show that the sensor's resonant frequency was 3.07 GHz. This frequency was set so that the resonator arrangement has two sensing areas, each dominated by either the electric or magnetic field. As is widely known, the size of the patch determines the resonant frequency [24]; similarly, the overall resonator length in this sensor determines the operating frequency.

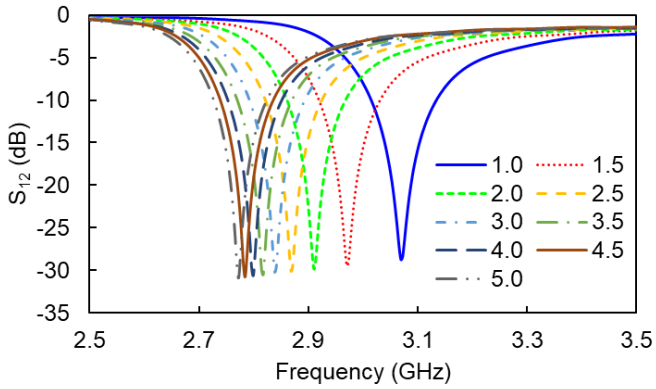


(a)

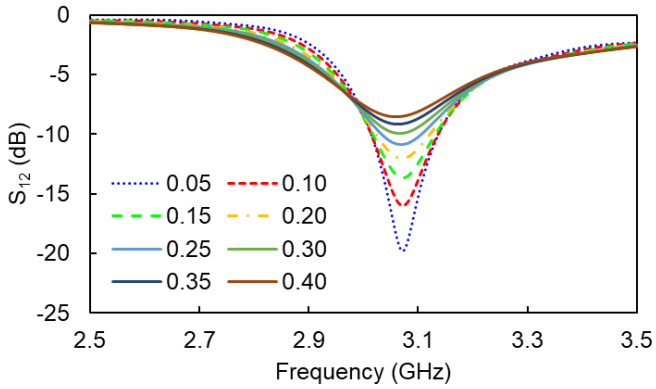


(b)

Figure 6. $S_{12}$ response to changes in (a) $\mu_r$ and (b) *tan* $\delta_m$ in MUT placed in the high H-field area

### 3.2 Mathematical Formulation

From the above results, the resonant frequency and Q-factor shifts of each sampling were recorded and arranged in graphical form. The resonant frequency data were normalized to the initial sensor frequency before the MUT was introduced, and the Q-factor data were similarly normalized to the initial sensor Q-factor. These data were then input into the curve-fitting toolbox [25] to derive equations based on the curves formed from the simulation data.

The curve-fitting feature offers several equation types, including linear, exponential, Fourier, Gaussian, and rational, to match the generated formula with the data curve. In this experiment, the equation that best fit the simulation data curves was a rational model, which uses constants with powers in the numerator and denominator. The sum of the powers of each parameter differs depending on the lowest sum of square error (SSE) value obtained from the curve-fitting results. Each value of $\varepsilon_r$, $\mu_r$, $tan\ \delta_e$, and $tan\ \delta_m$ is formulated by the equations written in Eq. (1) to (4).

$$\varepsilon_r = \frac{-4.216\left(\frac{f_{MUT}}{f_{un}}\right)^2 + 7.857\left(\frac{f_{MUT}}{f_{un}}\right) - 3.558}{\left(\frac{f_{MUT}}{f_{un}}\right)^2 - 1.409\left(\frac{f_{MUT}}{f_{un}}\right) + 0.4926} \quad (1)$$

$$\tan\delta_e = -5.016\left(\frac{Q_{un}}{Q_{MUT}}\right)^3 + 16.32\left(\frac{Q_{un}}{Q_{MUT}}\right)^2 - 16.89\left(\frac{Q_{un}}{Q_{MUT}}\right) + 5.59 \quad (2)$$

$$\mu_r = \frac{2.036\left(\frac{f_{MUT}}{f_{un}}\right)^2 - 4.636\left(\frac{f_{MUT}}{f_{un}}\right) + 2.74}{\left(\frac{f_{MUT}}{f_{un}}\right) - 0.8606} \quad (3)$$

$$\tan\delta_m = 2.98\left(\frac{Q_{un}}{Q_{MUT}}\right)^3 - 9.519\left(\frac{Q_{un}}{Q_{MUT}}\right)^2 + 10.85\left(\frac{Q_{un}}{Q_{MUT}}\right) - 4.312 \quad (4)$$

The notations $f_{MUT}$, $f_{un}$, $Q_{MUT}$, and $Q_{un}$ represent the resonant frequency of the MUT, the sensor frequency without the MUT, the Q-factor of the MUT, and the Q-factor of the sensor without the MUT, respectively. The $f_{un}$ and $Q_{un}$ values for the sensor were 3.07 GHz and 7.22, respectively. The extraction ratio curve comparing the CST simulation results and the formula from the curve-fitting is shown in Fig. 7. The blue dots represent data obtained from the CST simulation, while the red line represents the calculated parameters from the proposed formula.

Based on Fig. 7, the curve-fitting formula results align well with the simulated results. Figure 7a shows the extraction results for electrical characteristics, including $\varepsilon_r$ and $tan\ \delta_e$, while Figure 7b shows the extraction results for magnetic characteristics, including $\mu_r$ and $tan\ \delta_m$. These results indicate that Eq. (1) to (4) are appropriate equations for estimating relative permittivity ($\varepsilon_r$), permeability ($\mu_r$), dielectric loss ($tan\ \delta_e$), and magnetic loss ($tan\ \delta_m$).

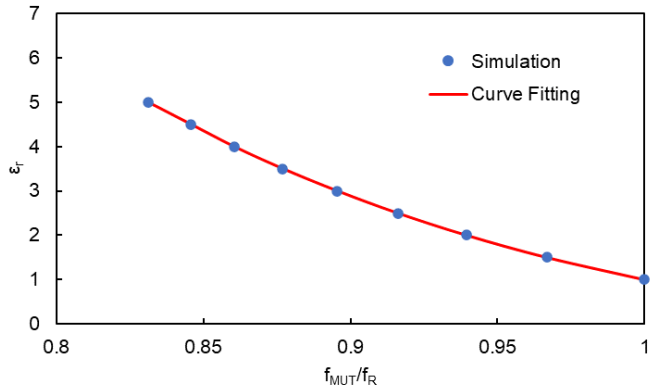
Simulation
Curve Fitting
εr
fMUT/fR

(a)

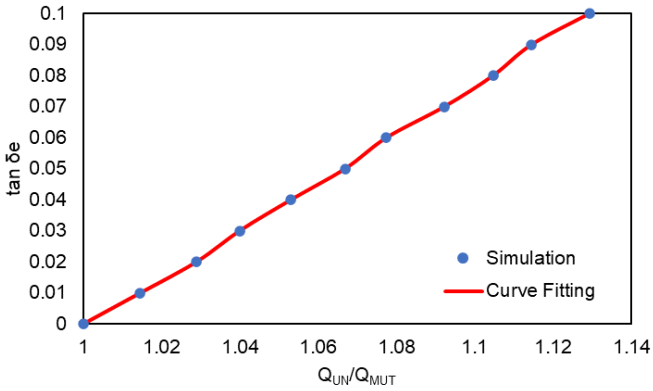
Simulation
Curve Fitting
tan δe
QUN/QMUT

(b)

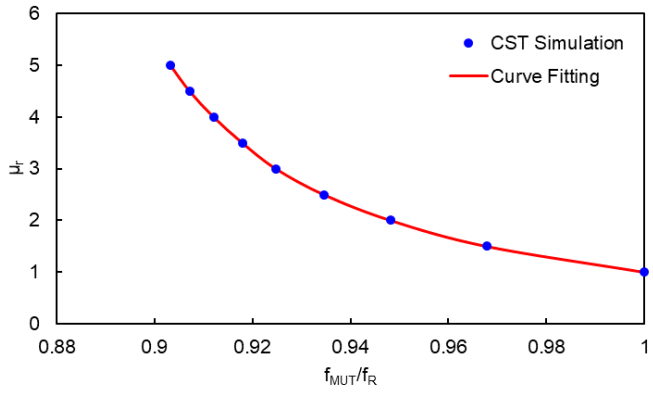
CST Simulation
Curve Fitting
μr
fMUT/fR

(c)

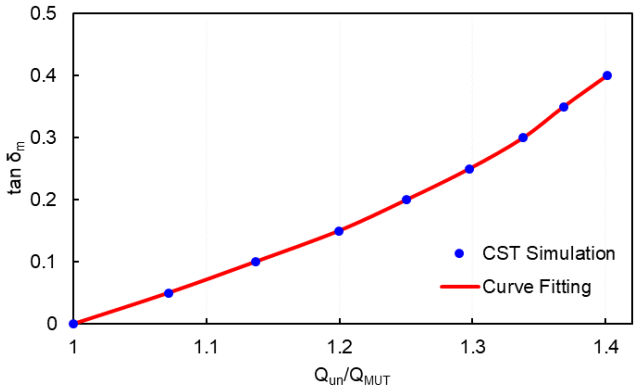


(d)

Figure 7. Comparison of the CST simulation results with the curve-fitting formula for the parameters: (a) $\varepsilon_r$, (b) *tan* $\delta_e$, (c) $\mu_r$, (d) *tan* $\delta_m$

To provide a clearer understanding of the advantages of our proposed method compared to other computational methods in electromagnetic simulation, we have compiled a comprehensive comparison, as seen in Table 1. This table includes key parameters, such as accuracy, processing time, and the advantages and disadvantages of its method.

Table 1. Comparison of Computational Method in EM Simulation

| No | Method | Accuracy | Processing time | Characteristics | Ref. |
|---|---|---|---|---|---|
| 1. | FDTD (Finite-Difference Time-Domain) | High | Medium | Suitable for analyzing EM wave propagation, modeling complex EM devices with high accuracy, and effectively handling varying spatial and temporal domains. **Cons**: Tradeoff Between Stability and Accuracy | [26]–[28], This work |
| 2. | MoM (Method of Moments) | High | Long | Effective for analyzing antennas and conductive structures, efficient for modeling electrical and EM structures with high accuracy, and suitable for modeling low to mid-frequency ranges. **Cons**: High computational cost over a wide freq. range | [29]–[31] |
| 3. | FEM (Finite Element Method) | High | Varies (depending on the model | Flexibility in modeling physical phenomena, accurate for HF modeling, enables the modeling of | [32]–[34] |

| | |
|---|---|
| complexity) | complex structures.<br>**Cons**: Need for expertise in setting up and interpreting simulation results |

## 4. CONCLUSION

The presence of new materials with unknown properties and characteristics is no longer a critical issue. Various methods can determine these materials' properties and characteristics, particularly regarding their electromagnetic behavior. One effective approach is utilizing a microstrip sensor, where the structure is sensitive to changes in material properties. Frequency shifts and Q-factor changes provide the basis for estimating the values of dielectric and magnetic properties. Based on the simulation results and mathematical matching, the proposed microstrip sensor successfully measures permittivity, permeability, dielectric loss, and magnetic loss. The experimental results of variations in relative permittivity ($\varepsilon_r$), dielectric loss ($tan\ \delta_e$), relative permeability ($\mu_r$), and magnetic loss ($tan\ \delta_m$), across nine samples each show conformity with the calculated results using the outlined formulas. Thus, the estimation results generated by these formulas based on the value of $S_{21}$ can be used to predict the actual material properties. Moreover, because this sensor can identify both magnetic and dielectric characteristics simultaneously, it excels in measuring the characteristics of magneto-dielectric materials.

## REFERENCES

[1] J. Kim, R. Kumar, A. J. Bandodkar, and J. Wang, "Advanced materials for printed wearable electrochemical devices: A review," *Adv. Electron. Mater.*, vol. 3, no. 1, p. 1600260, 2017.

[2] A. Afif, S. M. H. Rahman, A. T. Azad, J. Zaini, M. A. Islan, and A. K. Azad, "Advanced materials and technologies for hybrid supercapacitors for energy storage–A review," *J. Energy Storage*, vol. 25, p. 100852, 2019.

[3] W. Chiang, D. Mariotti, R. M. Sankaran, J. G. Eden, and K. (Ken) Ostrikov, "Microplasmas for Advanced Materials and Devices," *Adv. Mater.*, vol. 32, no. 18, p. 1905508, May 2020.

[4] Y. G. Adhiyoga, S. F. Rahman, C. Apriono, and E. T. Rahardjo, "Magneto-dielectric properties of PDMS–magnetite composite as a candidate for compact microstrip antennas in the C-band 5G frequency," *J. Mater. Sci. Mater. Electron.*, vol. 32, no. 8, pp. 11312–11325, 2021.

[5] Q. Peng *et al.*, "New materials graphyne, graphdiyne, graphone, and graphane: review of properties, synthesis, and application in nanotechnology," *Nanotechnol. Sci. Appl.*, vol. 7, p. 1, Apr. 2014.

[6] S. P. Sreenilayam, I. U. Ahad, V. Nicolosi, V. Acinas Garzon, and D. Brabazon, "Advanced materials of printed wearables for physiological parameter monitoring," *Mater. Today*, vol. 32, pp. 147–177, Jan. 2020.

[7] M. Jaroszewski, S. Thomas, and A. V Rane, *Advanced materials for electromagnetic shielding: fundamentals, properties, and applications*. John Wiley & Sons, 2018.

[8] H. S. Roslan, M. Alice Meor Said, Z. Zakaria, and M. H. Misran, "Recent development of planar microwave sensor for material characterization of solid, liquid, and powder: a review," *Bull. Electr. Eng. Informatics*, vol. 11, no. 4, pp. 1911–1918, Aug. 2022.

[9] M. Khairy Ismail, Z. Zakaria, N. Hassan, S. Weng Yik, and M. Mawardy Abdullah, "Microwave Planar Sensor for Determination of the Permittivity of Dielectric Material," *Bull. Electr. Eng. Informatics*, vol. 7, no. 4, pp. 640–649, Dec. 2018.

[10] N. Abd Rahman, Z. Zakaria, R. Abd Rahim, Y. Dasril, and A. A. Mohd Bahar, "Planar

Microwave Sensors for Accurate Measurement of Material Characterization: A Review," *TELKOMNIKA (Telecommunication Comput. Electron. Control.*, vol. 15, no. 3, p. 1108, Sep. 2017.

[11] M. T. Khan and S. M. Ali, "A brief review of measuring techniques for characterization of dielectric materials," *Int. J. Inf. Technol. Electr. Eng.*, vol. 1, no. 1, 2012.

[12] S. Santhanam and T. S. Palavesam, "Comparative characterization of microstrip patch antenna array with defected ground structure for biomedical application," *Bull. Electr. Eng. Informatics*, vol. 11, no. 1, pp. 346–353, Feb. 2022.

[13] M. Ibrahim, R. Abd Rahim, J. Mohd Nordin, S. Z. Abdul Nyzam, and N. Amira Amatkhri, "Dielectric properties characterization of the rice and rice weevil for microwave heating treatment," *Indones. J. Electr. Eng. Comput. Sci.*, vol. 13, no. 2, p. 752, Feb. 2019.

[14] S. Subbaraj, V. S. Ramalingam, M. Kanagasabai, E. F. Sundarsingh, Y. P. Selvam, and S. Kingsley, "Electromagnetic Nondestructive Material Characterization of Dielectrics Using EBG Based Planar Transmission Line Sensor," *IEEE Sens. J.*, vol. 16, no. 19, pp. 7081–7087, Oct. 2016.

[15] A. Ebrahimi, J. Scott, and K. Ghorbani, "Transmission Lines Terminated With LC Resonators for Differential Permittivity Sensing," *IEEE Microw. Wirel. Components Lett.*, vol. 28, no. 12, pp. 1149–1151, Dec. 2018.

[16] I. Piekarz, J. Sorocki, K. Wincza, and S. Gruszczynski, "Liquids Permittivity Measurement Using Two-Wire Transmission Line Sensor," *IEEE Sens. J.*, vol. 18, no. 18, pp. 7458–7466, Sep. 2018.

[17] O. J. Famoriji and T. Shongwe, "Transmission line characterization and modeling for electronic circuits and systems design," *Indones. J. Electr. Eng. Comput. Sci.*, vol. 30, no. 2, p. 730, May 2023.

[18] S. Alam, Z. Zakaria, I. Surjati, N. A. Shairi, M. Alaydrus, and T. Firmansyah, "Integrated Microwave Sensor and Antenna Sensor Based on Dual T-Shaped Resonator Structures for Contact and Noncontact Characterization of Solid Material," *IEEE Sens. J.*, vol. 23, no. 12, pp. 13010–13018, 2023.

[19] S. Alam, Z. Zakaria, I. Surjati, N. A. Shairi, M. Alaydrus, and T. Firmansyah, "Multifunctional of dual-band permittivity sensors with antenna using multicascode T-shaped resonators for simultaneous measurement of solid materials and data transfer capabilities," *Measurement*, vol. 217, p. 113078, 2023.

[20] Y. G. Adhiyoga, S. F. Rahman, C. Apriono, and E. T. Rahardjo, "Miniaturized 5G Antenna With Enhanced Gain by Using Stacked Structure of Split-Ring Resonator Array and Magneto-Dielectric Composite Material," *IEEE Access*, vol. 10, pp. 35876–35887, 2022.

[21] M. Saadat-Safa, V. Nayyeri, M. Khanjarian, M. Soleimani, and O. M. Ramahi, "A CSRR-Based Sensor for Full Characterization of Magneto-Dielectric Materials," *IEEE Trans. Microw. Theory Tech.*, vol. 67, no. 2, pp. 806–814, 2019.

[22] H. Sun, T. Tang, and G. Du, "Improved approach using symmetric microstrip sensor for accurate measurement of complex permittivity," *Int. J. RF Microw. Comput. Eng.*, vol. 28, no. 5, p. e21258, Jun. 2018.

[23] H. Amar, H. Ghodbane, M. Amir, M. A. Zidane, C. Hamouda, and A. Rouane, "Microstrip sensor for product quality monitoring," *J. Comput. Electron.*, vol. 19, no. 3, pp. 1329–1336, 2020.

[24] H. Wheeler, "Small antennas," *IEEE Trans. Antennas Propag.*, vol. 23, no. 4, pp. 462–469, Jul. 1975.

[25] S. Machluf, "Curve fitting in Matlab," *Retrieved Sept.*, vol. 9, p. 2014, 2008.

[26] J. Shibayama, A. Kawahara, J. Yamauchi, and H. Nakano, "Frequency-dependent finite-difference time-domain method based on iterated Crank–Nicolson scheme," *Electron. Lett.*, vol. 59, no. 1, p. e12695, Jan. 2023.

[27] R. M. S. de Oliveira and R. R. Paiva, "Least Squares Finite-Difference Time-Domain," *IEEE Trans. Antennas Propag.*, vol. 69, no. 9, pp. 6111–6115, 2021.

[28] J. Wang and Q. Ren, "A 3-D Hybrid Maxwell's Equations Finite-Difference Time-Domain (ME-FDTD)/Wave Equation Finite-Element Time-Domain (WE-FETD) Method," *IEEE Trans. Antennas Propag.*, vol. 71, no. 6, pp. 5212–5220, 2023.

[29] A. Alhaj Hasan, T. M. Nguyen, S. P. Kuksenko, and T. R. Gazizov, "Wire-Grid and Sparse

MoM Antennas: Past Evolution, Present Implementation, and Future Possibilities," *Symmetry*, vol. 15, no. 2. 2023.

[30] H.-B. Yuan, W.-T. Bao, C. H. Lee, B. F. Zinser, S. Campione, and J.-F. Lee, "A Method of Moments Wide Band Adaptive Rational Interpolation Method for High-Quality Factor Resonant Cavities," *IEEE Trans. Antennas Propag.*, vol. 70, no. 5, pp. 3595–3604, 2022.

[31] Y. Gao, M. F. Akbar, and G. N. Jawad, "Stabilized and Fast Method for Compressive-Sensing-Based Method of Moments," *IEEE Antennas Wirel. Propag. Lett.*, vol. 22, no. 12, pp. 2915–2919, 2023.

[32] A. J. Bracamonte, V. Mercado-Puche, G. Martínez-Arguelles, L. F. Pumarejo, A. R. Ortiz, and L. C. Herazo, "Effect of Finite Element Method (FEM) Mesh Size on the Estimation of Concrete Stress–Strain Parameters," *Applied Sciences*, vol. 13, no. 4. 2023.

[33] B. Stupfel, P. Andrieu, M. Lecouvez, and A. Pujols, "Efficient Feed Port Modeling of Patch or Microstrip Antennas in a Finite-Element Method," *IEEE Trans. Antennas Propag.*, vol. 71, no. 12, pp. 9386–9393, 2023.

[34] N. Xu, X. Wang, D. Lin, and W. Zuo, "Numerical Simulation and Optimization of Screening Process for Vibrating Flip-Flow Screen Based on Discrete Element Method–Finite Element Method–Multi-Body Dynamics Coupling Method," *Minerals*, vol. 14, no. 3. 2024.